

Received December 16, 2019, accepted December 26, 2019, date of publication December 30, 2019, date of current version January 7, 2020.

Digital Object Identifier 10.1109/ACCESS.2019.2962967

# Cross-Coupled Repetitive Control of a Compliant Nanomanipulator for Micro-Stereolithography

YUE CAO<sup>1</sup>, (Student Member, IEEE), AND ZHEN ZHANG<sup>1,2</sup>, (Member, IEEE)

<sup>1</sup>State Key Laboratory of Tribology, Department of Mechanical Engineering, Institute of Manufacturing Engineering, Tsinghua University, Beijing 100084, China

<sup>2</sup>Beijing Key Laboratory of Precision/Ultra-Precision Manufacturing Equipment and Control, Tsinghua University, Beijing 100084, China

Corresponding author: Zhen Zhang (zzhang@tsinghua.edu.cn)

This work was supported in part by the National Natural Science Foundation of China under Grant 51875313, and in part by the Open Foundation of the State Key Laboratory of Tribology, Institute of Manufacturing Engineering, under Grant SKLT2019C09.

**ABSTRACT** This paper proposes an easy-implemented and high precision contouring control method for a self-developed compliant nanomanipulator supporting cost-effective micro-stereolithography (MSL). The proposed contouring control method is composed of a repetitive controller (RC) to achieve periodic trajectory tracking for each axis, and a cross-coupled control (CCC) for the coordination of contour errors. It is worth noting that the cross-coupled controller design and its integration to RC are not straightforward, as an incorrect feedback position may even deteriorate the contouring and an inappropriate design of the cross-coupled controller leads to instability of the system. For the proposed control structure, a correct feedback position is designed, hence a cross-coupled controller is constructed to ensure the stability and contour error reduction. Various simulations and real-time experiments are deployed on the nanomanipulator, and the comparative results validate the enhanced contour tracking performance of the proposed control method with the contour error 86 nm.

**INDEX TERMS** Contouring control, nano-positioning, mechatronics, tracking, micro-stereolithography.

## I. INTRODUCTION

Additive manufacturing (AM) is a process allowing the rapid production of varied-size models and prototypes, and the manufacturing is implemented based on a layer-by-layer process. As one kind of scalable AM techniques, micro-stereolithography (MSL) [1], [2] is stereolithography in microscale, which represents a promising method owing to high resolution and repeatability. MSL processes have been widely applied to many areas, such as biomaterial scaffold [3], implant organs [4] and microfluidic devices [5]. With the development of MSL, more stringent fabrication demands are posed. For example, a micro-tweezer proposed in [6] requires  $2\mu\text{m}$  accuracy and  $400\mu\text{m}$  working range, and a microscopic four-point probe of a microsensors [7] requires 200nm accuracy and 10mm working range.

To further improve the fabrication quality, MSL systems based on the two-photon polymerization process were developed in [8], [9], of which the accuracy reached around 100 nm. Nevertheless, the two-photon polymerization process requires costly laser source and complicated

optical systems. In addition, the nonlinearity of the photopolymer was utilized to improve the accuracy of MSL processes [10], [11], where the wavelength of the laser source was restrictive. The commonly applicable UV laser sources are also of high cost. Recent result suggested that commercialized products such as Blu-ray optical unit [12] can be utilized as a light source to achieve high fabrication quality at low cost.

Besides the optical systems, MSL process requires continuous motion during the fabrication in one layer, hence the dynamics of the XY motion system is very important to achieve high precision motion quality. Most existing results of MSL (e.g. [13]) utilized commercial contact bearing based motion stages, which restrict them at submicrons level motion quality. Moreover it is difficult to interfere in the drivers of commercial motion stages, so the system dynamics cannot be dealt with by self-designed control methods for specific contouring conditions.

To tackle the above challenges of costly laser source and closed-architecture motion stage, we propose an MSL prototype (FIGURE 1(a)) by means of a self-developed nanomanipulator and a cost-effective light emitting diode (LED) module, enabling nanometric accuracy fabrication and

The associate editor coordinating the review of this manuscript and approving it for publication was Hassen Ouakad<sup>1</sup>.

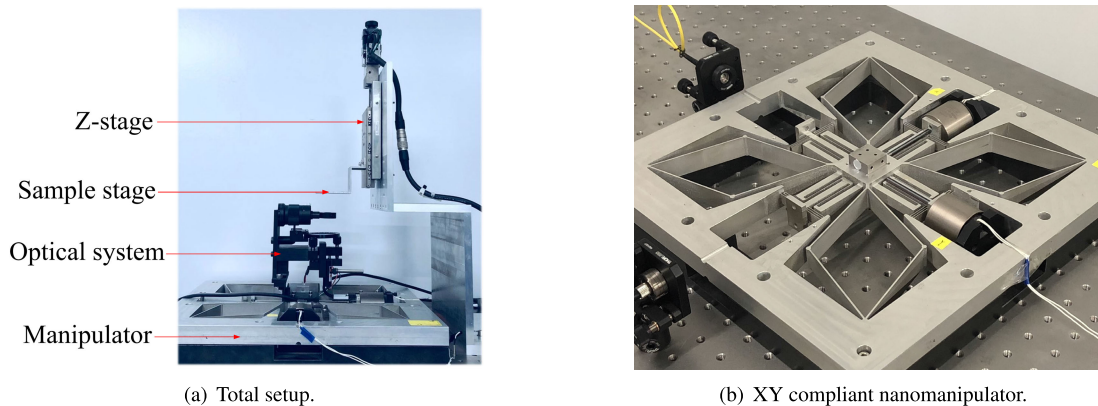


**FIGURE 1. A compliant nanomanipulator-based MSL system.**

single-digit micron feature size of free form contours via the nanomanipulator and photopolymer nonlinearity effect, respectively. The MSL system utilized the fixed surface method [14], by which the sample is fixed and immersed in a polymer resin and mounted on a Z-axis motion stage while a cost-effective 405 nm LED module is mounted on an XY compliant motion stage as the light source. The detailed description of the MSL system is referred to [15].

Since an MSL is operated by a layer-by-layer fashion, it is crucial to have a precision contouring control in each layer. Then 3D microfabrication can be obtained by step motion along Z axis. Clearly, the quality microfabrication is dependent of both the mechanical design (which will be discussed in Section II) of the XY motion stage and its contouring control.

Note that contouring control of multi-axis motion system can be mainly classified by the following types: 1) the cross-coupled control (CCC), in which the contour error is estimated and fed back based on axial tracking errors; 2) the position domain control (PDC) [16], [17], in which the system is considered as a master-slave one, and only the slave axis needs to be controlled in position domain to reduce the contour error; 3) the task coordinate frame (TCF) based contouring control, including local task coordinate frame (LTCF) [18] and its optimization global task coordinate frame (GTCF) [19], [20], in which both the contour error and axial tracking error are dealt with in the position domain. Among these methods, CCC is most widely used due to its simplicity for integration and implementation. In the literature, the axial tracking controller in CCC is usually a PID-based one with either a constant or variable gain [21]. Clearly if the axial tracking error can be further improved, then the resulting contour error of that combined with CCC can be improved as well. For the combination of CCC and axial tracking controllers, such as cross-coupled adaptive control [22], fuzzy control [23], and iterative learning control [24]. Nevertheless fuzzy control [25] and adaptive control [26] are mainly focused on the robustness of the control system. While the aim of this work is to achieve a high precision microfabrication based on a self-developed motion system.

Note that a closed contour can be generated by periodic trajectories of each axis. Also it is known that repetitive control (RC) is effective to deal with periodic signals for linear time-invariant (LTI) systems. Compared with RC, iterative learning control (ILC) deals with repetitive tasks in a multi-trail fashion. Nevertheless, the tracking error of ILC may not asymptotically converge in practice due to measurement errors coinciding with iteration errors. Moreover, an unclosed contour can be made to a closed one via adding the corresponding portion (which is not actually fabricated by controlling the laser source via a shutter) and then repeat. By this way, RC can then be applied. This motivates us to investigate an integrated structure of RC and CCC to improve the contouring performance for repetitive contouring in this work. Moreover, RC is a time domain controller, so it is difficult to integrate RC and the position domain controllers such as PDC and GTCF as well as to analyze the stability of the integrated system. Therefore, we, in this work, concentrate on the integration of RC and CCC and the stability analysis of the integrated structure for repetitive contours.

A preliminary version of this work was presented in the 2018 Chinese Control Conference [27]. And this paper expands the investigation with modified theoretical analysis and experimental results. The main contributions of this paper are as follows:

1. An easy-implemented and high precision contouring control structure is proposed for a self-developed compliant nanomanipulator supporting a cost-effective MSL system.
2. For the proposed RC-CCC control structure, a correct feedback position is designed, hence a cross-coupled controller is constructed to ensure the stability and contour error reduction.
3. The effectiveness of the proposed RC-CCC method is validated by numerous comparative experiments, including repetitive circular, goggle-shaped, and heart-shape contours.

The rest of the paper is organized as follows: in Section II the dynamic model of the plant under consideration

is discussed. An integrated structure of RC and CCC is proposed in Section III. Then numerous simulations and real-time experiments are conducted on a compliant nanomanipulator, and comparative results show the effectiveness of the proposed control method for contouring control in Section IV, followed by conclusion in Section V.

## II. MODELING OF A COMPLIANT NANOMANIPULATOR

For the mechanical design of the XY motion stage in the MSL system, a self-developed XY compliant nanomanipulator (FIGURE 1(b)) is utilized, thanks to its nanoprecision by using non-contact bearings which avoid friction and backlash. Moreover, flexure bearings are maintenance free and the compliant manipulator can be monolithically fabricated to avoid assembly. To actuate the nanomanipulator, each axis is equipped with a voice coil motor (VCM) and guided by flexure bearings. Two VCMs (BEI-Kimco Magnetics, Vista, CA, USA) are utilized, of which the stroke, peak and continuous force are  $\pm 3.1\text{mm}$ ,  $89\text{N}$  and  $24.5\text{N}$ , respectively. And the detailed mechanical design is referred to [28].

To achieve nanoprecision control of the above self-developed XY nanomanipulator, we consider its dynamic model within a relatively small stroke ( $\pm 100\mu\text{m} \times \pm 100\mu\text{m}$ ). By design, each axial dynamics can be modeled as a linear system of the following form

$$P(z^{-1}) = P_n(z^{-1}) (1 + \Delta(z^{-1})), \quad (1)$$

where  $z^{-1}$  represents the unit delay. The unmodeled dynamics  $\Delta(z^{-1})$  is stable, and the nominal plant model  $P_n(z^{-1})$  can be modeled as

$$P_n(z^{-1}) = \frac{z^{-r} B_p^c(z^{-1}) B_p^u(z^{-1})}{A_p(z^{-1})}, \quad (2)$$

where  $A_p(z^{-1})$  is the denominator of the transfer function  $P_n(z^{-1})$ , and  $B_p^c(z^{-1})$  and  $B_p^u(z^{-1})$  are the nominator of  $P_n(z^{-1})$  with stable and unstable zeros respectively, and  $r$  is the relative degree of  $P_n(z^{-1})$ .

With above plant dynamics, we would like to propose a contouring control method, which is capable of achieving enhanced contour precision and is easy to be implemented. For this reason, we consider an integrated contouring control architecture, which will be presented in the following section.

## III. CONTOURING CONTROL DESIGN

In this section, we propose a control structure to achieve contouring control by integrating CCC and RC. Note that the integration is not trivial. It is because that the feedback position of contour errors affects the contouring performance, also a cross coupled controller needs to be carefully designed to ensure the stability of the coupled control structure. In what follows, we recall the existing results of the CCC and discuss the crucial points of the integration of CCC and RC, which is one of the contributions of this work.

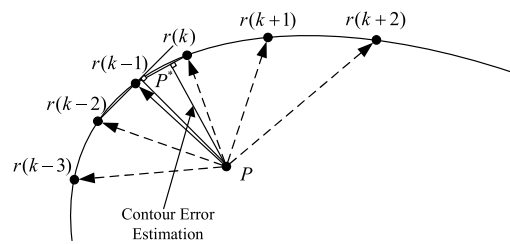


FIGURE 2. Schematic of GCCC contour error calculation.

### A. PRELIMINARIES OF CROSS-COUPLED CONTROL

To deal with regular contours, such as lines and circles, the CCC (constant or variable) [21], [29] was proposed to calculate the contour error by synthesizing axial errors. Then the contour error goes through a controller  $C$ , and then is assigned to each axial control input. Hence, the contour error can be calculated by

$$\varepsilon = -C_x e_x + C_y e_y, \quad (3)$$

where for lines,

$$C_x = \sin \theta, \quad C_y = \cos \theta, \quad (4)$$

and for circles,

$$C_x = \sin \theta - \frac{e_x}{2R}, \quad C_y = \cos \theta + \frac{e_y}{2R}. \quad (5)$$

Further the generalized cross-coupled control (GCCC) [30] was proposed to deal with free form contours, and the idea of the contour error calculation by GCCC is shown in FIGURE 2, where  $P$  is the current tracking position, and  $r(k)$  is the current reference position. Note that in this work the references are discrete and are constructed by a series of points, which are generated by sampling from the B-spline curves offline. The contour error can be calculated by the following algorithm.

---

#### Algorithm 1 Contour Error Calculation of GCCC

---

- (1) From the reference positions  $r(k - N)$  to  $r(k + N)$ , determine the closest one to the current position  $P$ , then denote it by  $r(m)$ ;
  - (2) Denote the line connecting  $r(m)$  and  $r(m - 1)$  by Line 1, and the line connecting  $r(m)$  and  $r(m + 1)$  by Line 2;
  - (3) Denote the feet of perpendicular from  $P$  to Line 1 and Line 2 by  $P_1$  and  $P_2$  respectively;
  - (4) The contour error  $\varepsilon$  of position  $P$  can be determined by  $\varepsilon = \min\{PP_1, PP_2\}$ .
- 

With the above calculation of the contour error, the contouring control of GCCC can be similarly designed to that of CCC structure. It is left to show the integration of CCC and RC, which is the main concern of this work and will be discussed in the next subsection.

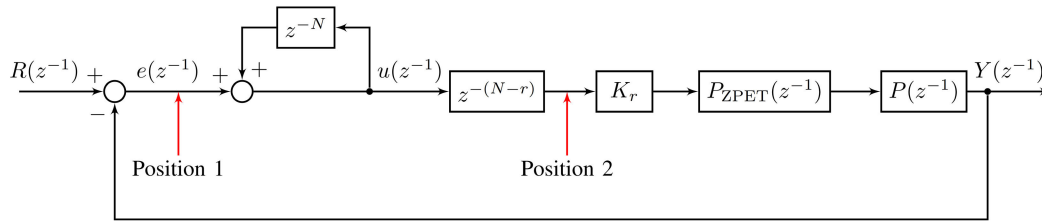


FIGURE 3. Block diagram of the axial RC structure.

**B. PROPOSED RC-CCC CONTROL METHOD**

Note that for the existing CCC structures in the literature, axial tracking is dealt with by PID-based controllers, and hence there is no need to consider the contour error feedback positions. Whereas if the RC is invoked instead of PID, then a delay process will be introduced to axial controllers. Thus the feedback position of the contour errors becomes important to the design in the presence of the delay process. Or in other words, if the feedback position is not correctly designed, the RC-CCC structure might even deteriorate the contouring performance.

In specific, to control the contour error in real-time, the axial outputs are required to be adjusted by the contour error feedback in  $r$  sampling steps ( $r$  is the relative degree), otherwise the axial outputs and contour error are not synchronized i.e. the sampling instants are different. That is why one needs to analyze the delay block of RC structure shown in FIGURE 3, where it reads as

$$u(z^{-1}) = z^{-N}u(z^{-1}) + e(z^{-1}). \tag{6}$$

And equation (6) can be expressed in time domain as

$$\begin{aligned} u(k) &= u(k - N) + e(k) \\ &= e(k) + e(k - N) + e(k - 2N) + \dots \end{aligned} \tag{7}$$

Also signal  $u(z^{-1})$  needs to go through the delay process  $z^{-(N-r)}$ . Equation (7) shows that in the RC, the error is accumulated once every  $N$  samples, and this summation will not be output until it goes through another  $(N - r)$ -sampling period delay. FIGURE 3 shows two feedback positions physically implementable. For Position 1, the axial output will not be affected by the feedback contour error until  $(N - r)$  samples later. Hence the controller cannot change the contour error in real-time. In contrast, for Position 2, the axial output  $Y(z^{-1})$  of a contour error feedback  $F(z^{-1})$  reads as

$$Y(z^{-1}) = K_r P_{ZPET}(z^{-1}) P(z^{-1}) \cdot F(z^{-1}), \tag{8}$$

where the Zero Phase Error Tracking (ZPET) controller  $P_{ZPET}(z^{-1})$  is of the form

$$P_{ZPET}(z^{-1}) = \frac{A_p(z^{-1})B_p^u(z)}{bB_p^c(z^{-1})}, \tag{9}$$

with a control gain  $b \geq \max |B^-(e^{-j\omega})|^2$ , for all  $\omega \in [0, \pi]$ , and a control gain  $K_r$  is ranging over  $(0, 2)$  to ensure the closed-loop stability.

Notice that the axial output can be adjusted by the contour error feedback in real-time, so Position 2 is chosen as the contour error feedback position of the integrated RC-CCC structure.

With this, we propose an integrated structure of RC and CCC as shown in FIGURE 4. Likewise, the integrated structure of RC and GCCC can be proposed as well except for replacing controller  $C$  in FIGURE 4 by Algorithm 1. And the corresponding control block diagram is omitted due to the similarity.

The robust RC is designed as follows

$$G_r(z^{-1}) = \frac{K_r z^{-N+r} q(z, z^{-1}) A_p(z^{-1}) B_p^u(z)}{[1 - q(z, z^{-1}) z^{-N}] b B_p^c(z^{-1})}, \tag{10}$$

where a low-pass filter  $q$  is designed to achieve robust stability. Furthermore, to reduce non-periodic disturbances, a modified repetitive control (MRC) [31] was provided, which utilized another filter  $Q$  to achieve full-band disturbance rejection capacity. Filter  $Q$  is designed by the following equation:

$$1 - z^{-r} Q(z^{-1}) = \frac{1 - z^{-N}}{1 - \alpha^N z^{-N}}, \tag{11}$$

where  $\alpha$  is a parameter varying in  $(0, 1)$ . In the following subsection, we provide the design of the cross coupled controller and the stability analysis of the RC-CCC system.

**C. STABILITY ANALYSIS OF THE INTEGRATED RC AND CCC**

The stability analysis of the proposed RC-CCC structure shown in FIGURE 4 is presented in the following theorem.

*Theorem 1: Considering the following cross coupled controller  $C$  of the form*

$$C(z^{-1}) = \frac{k_c \cdot W_x(z^{-1}) W_y(z^{-1})}{(C_x^2 + C_y^2)(1 - z^{-N})}, \tag{12}$$

where

$$W_i(z^{-1}) = z^{-N} [S_i(z^{-1}) - 1] + 1, \quad i = x, y, \tag{13}$$

$$S_i(z^{-1}) = \frac{K_{r_i} B_{p_i}^u(z) B_{p_i}^u(z^{-1})}{b_i}, \quad i = x, y, \tag{14}$$

if the control gain  $k_c$  satisfies  $0 < k_c < \frac{1}{4}$ , then the integrated RC and CCC system is stable.

The proof of Theorem 1 is referred to Appendix.

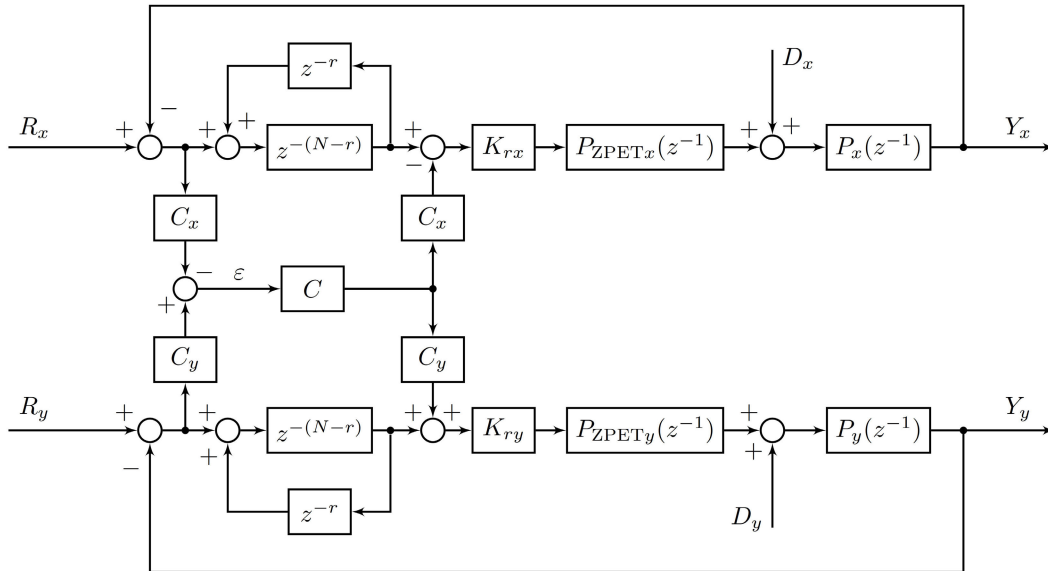


FIGURE 4. Block diagram of the proposed integrated structure of RC and CCC.

Note that the RC can be replaced by the MRC, and the CCC can be replaced by the GCCC, nevertheless the theoretical analysis becomes difficult due to the inexplicit controller form of GCCC. In what follows, we conduct numerous simulation and experimental scenarios to validate the proposed contouring control structure.

IV. SIMULATION AND EXPERIMENTAL RESULTS

Consider the XY nano-manipulating system, of which the identified transfer functions of X and Y axes are

$$P_{n_x}(z^{-1}) = \frac{z^{-1}(0.2731z^{-1} + 0.2746)}{z^{-2} - 1.9133z^{-1} + 1.0150} \quad (15)$$

and

$$P_{n_y}(z^{-1}) = \frac{z^{-1}(0.1596z^{-1} + 0.1606)}{z^{-2} - 1.9193z^{-1} + 1.0187}, \quad (16)$$

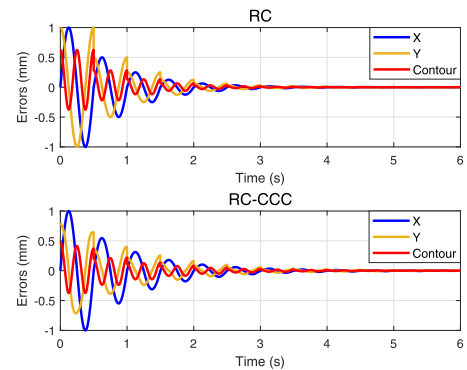
respectively, with a sampling period of 1 ms. Four case studies of different contouring control methods are investigated and the comparative results are shown in the following subsection.

A. SIMULATION RESULTS

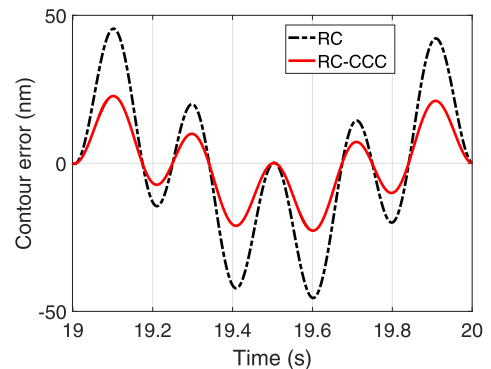
1) CASE I: INTEGRATED RC AND CCC

To simulate the fabrication process, a repetitive circular contour (a circle repeated by multiple times) was set with radius of  $R = 1$  mm, and frequency of  $\omega = 4\pi$  rad/s as the reference. For detailed parameters of controller  $C$ ,  $S_x$  and  $S_y$  are set as  $S_x = 1.67(0.15 + 0.075z + 0.075z^{-1})$  and  $S_y = 4.88(0.05 + 0.025z + 0.025z^{-1})$ , respectively,  $C_x$  and  $C_y$  are set according to equation (5), and  $N = 500$ ,  $k_c = 0.2$ .

Biaxial periodic disturbances were introduced with amplitude of  $5 \mu V$ , and frequency of  $\omega = 6\pi$  rad/s. The result



(a) Convergence of axial and contour errors.



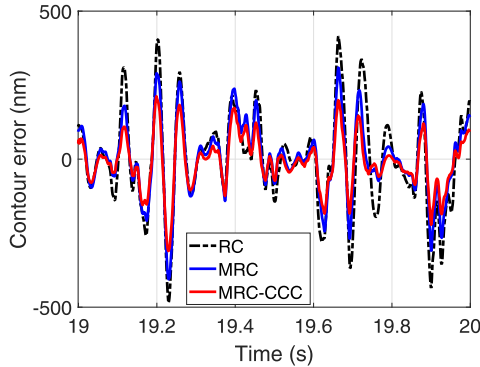
(b) Steady state contour errors.

FIGURE 5. Comparison of the RC-CCC and standalone RC in presence of periodic disturbance.

is shown in FIGURE 5(a) and 5(b). It is clearly seen that the axial and contour errors converge because of the RC structure. The steady state contour errors are shown in FIGURE 5(b)

**TABLE 1. Circular contour errors (RMS) of RC, RC-CCC and PID-CCC with different disturbances.**

Disturbances	RC (nm)	RC-CCC (nm)	PID-CCC (nm)
N/A	6.0e-9	4.5e-9	1821
A=5e-6 V, $\omega=4\pi$ rad/s	5.5e-9	4.2e-9	1821
A=5e-6 V, $\omega=6\pi$ rad/s	30	18	1821
A=5e-9 V, white noise	128	86	1821



**FIGURE 6. Comparison of RC, MRC and MRC-CCC in presence of white noise.**

**TABLE 2. Circular contour errors (RMS) of RC, MRC and MRC-CCC in presence of white noise disturbances.**

White noise disturbances	RC (nm)	MRC (nm)	MRC-CCC (nm)
A=5e-10 V	40	32	23
A=5e-9 V	128	101	69
A=5e-8 V	404	319	218

by zooming in FIGURE 5(a) (in the following results only steady state contour errors are provided). The simulation result shows that the integrated RC and CCC method significantly reduced the circular contour error comparing to the standalone RC in the presence of disturbances.

Then disturbances of different frequencies were conducted. The RMS values of the contour error were calculated and listed in TABLE 1. Specially, the disturbance of the same frequency as the reference was well rejected by RC. Furthermore, for disturbances with different frequencies, the RC-CCC structure is capable of significantly reducing circular contour errors, comparing to the standalone RC. Also the contour errors of the PID-based CCC are much larger than that of the RC-CCC. Therefore the proposed RC-CCC outperforms the PID-CCC for repetitive contours.

2) CASE II: INTEGRATED MRC AND CCC

In order to reject non-periodic disturbances, the RC was replaced by the MRC method, where the parameter is set as  $\alpha = 0.999$ . A white noise disturbance was considered.

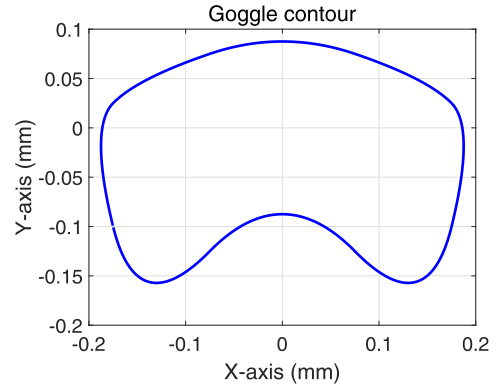


**FIGURE 7. Goggle contour.**

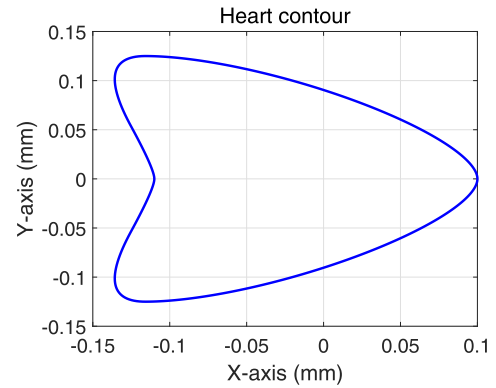


**FIGURE 8. Heart contour.**

**TABLE 3. Contour errors (RMS) of RC, RC-GCCC and PID-GCCC with different disturbances (G: goggle, H: heart).**

Disturbances	RC (nm)	RC-GCCC (nm)	PID-GCCC (nm)
N/A	G: 1.6e-9 H: 2.6e-9	G: 1.2e-9 H: 1.7e-9	G: 1139 H: 909
A=5e-6 V, $\omega=\pi$ rad/s	G: 25 H: 31	G: 13 H: 15	G: 1139 H: 909
A=5e-6 V, $\omega=7\pi$ rad/s	G: 26 H: 31	G: 14 H: 16	G: 1139 H: 909
A=5e-9 V, white noise	G: 131 H: 120	G: 74 H: 71	G: 1139 H: 909

It is shown in FIGURE 6 that the MRC method has a better ability of rejecting non-periodic disturbances comparing to RC method. Meanwhile, if the MRC is integrated with the CCC, the circular contour error can be further reduced comparing to standalone MRC. Further simulations with white noise disturbances at different amplitudes were also conducted and the results were listed in TABLE 2.

3) CASE III: INTEGRATED RC AND GCCC

We chose two free form contours used in [32]. These two contours were goggle contour (shown in FIGURE 7, with repetition period 0.667sec) and heart contour (shown in FIGURE 8, with repetition period 1sec). The GCCC structure is constructed by utilizing Algorithm 1.

**TABLE 4.** Contour errors (RMS) of RC, MRC and MRC-GCCC with white noise disturbances (G: goggle, H: heart).

White noise disturbances	RC (nm)	MRC (nm)	MRC-GCCC (nm)
A=5e-10 V	G: 41 H: 38	G: 32 H: 33	G: 20 H: 20
A=5e-9 V	G: 131 H: 120	G: 101 H: 103	G: 64 H: 64
A=5e-8 V	G: 413 H: 378	G: 318 H: 325	G: 202 H: 203

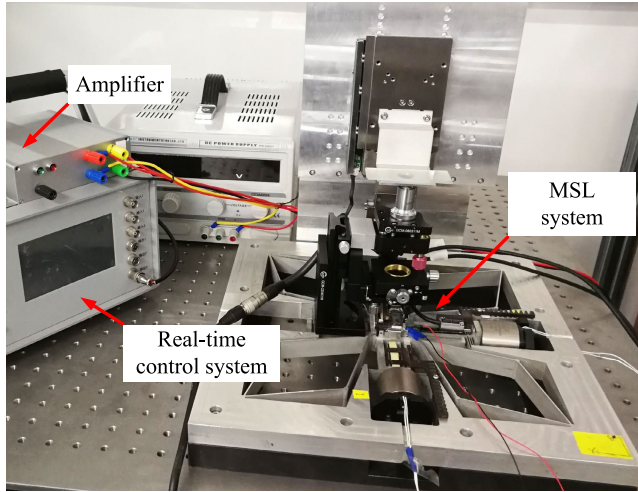


**FIGURE 9.** Experimental setup.

In TABLE 3, a comparison of contour errors of different control structures was conducted. It is shown in TABLE 3 that for the two free form contours in the presence of disturbances of different frequencies, the integrated RC and GCCC significantly reduced the contour error, comparing to the standalone RC. Also, the contour error of RC-GCCC is much smaller than that of PID-GCCC. Therefore the proposed RC-GCCC outperformed PID-GCCC for repetitive contours.

4) CASE IV: INTEGRATED MRC AND GCCC

For non-periodic disturbances, the RC was replaced by the MRC. It is shown in TABLE 4 that for the free form contours, the integrated MRC and GCCC can reduce the contour error comparing to the standalone RC and MRC.

**B. EXPERIMENTAL RESULTS**

In this subsection, the proposed RC-CCC method was real-time deployed on the self-developed compliant-nanomanipulator-based MSL system shown in FIGURE 9. The real-time control was conducted via a self-developed DSP servo board. Linear optical encoders were equipped on each axis for real-time displacement feedback with a resolution of 1.2 nm. The identified plant model of each axis in equations (15), (16) were used at a 1 kHz sampling frequency.

First of all, a repetitive circular reference of amplitude 0.1 mm and frequency 1 Hz was implemented. For detailed

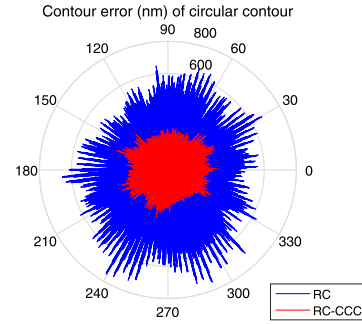


**FIGURE 10.** Experimental results of RC-CCC (reference amplitude 0.1 mm, frequency 1 Hz).

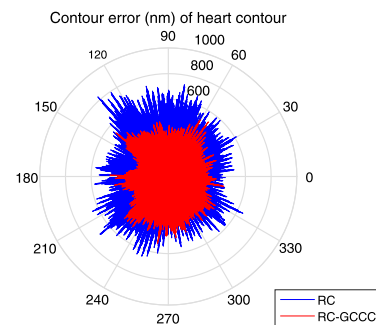
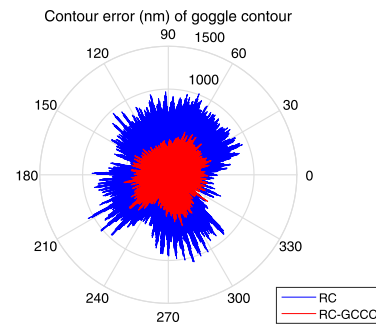


**FIGURE 11.** Experimental results of RC-GCCC (goggle contour (top), heart contour (bottom)).

parameters of controller  $C$ ,  $S_x$  and  $S_y$  are set as  $S_x = 0.00334(0.15 + 0.075z + 0.075z^{-1})$  and  $S_y = 0.00781(0.05 + 0.025z + 0.025z^{-1})$ , respectively,  $C_x$  and  $C_y$  are set according to equation (5), and  $N = 500$ ,  $k_c = 0.2$ .

A significant reduction of the contour error (plotted in the polar coordinates) by the CCC is observed in FIGURE 10. Then, repetitive goggle and heart references (with the same parameters as those in the simulations) were conducted via Algorithm 1 as well, and the significant reductions in contour errors (plotted in the polar coordinates) of GCCC are observed in FIGURE 11.

The comparison of the contour errors with RC of three types of references was summarized in TABLE 5, where significant contour error reductions are observed by the RC-CCC/GCCC comparing to the standalone RC.

Also we experimentally implemented the integrated MRC and CCC/GCCC structure to testify the capability of rejecting non-periodic disturbances. The MRC parameter is set as

TABLE 5. The experimental contour errors (nm) with RC.

Contour	RC	RC-CCC/GCCC	Error reduction
Circular contour	188.3	86.5	54.1%
Goggle contour	359.1	178.1	50.4%
Heart contour	209.4	153.8	26.6%

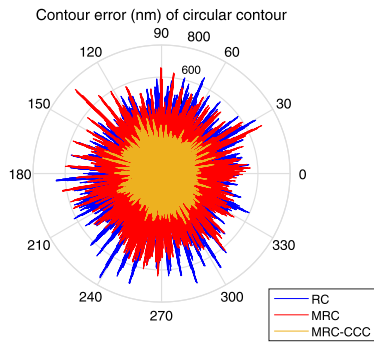


FIGURE 12. Experimental results of MRC-CCC (reference amplitude 0.1 mm, frequency 1 Hz).

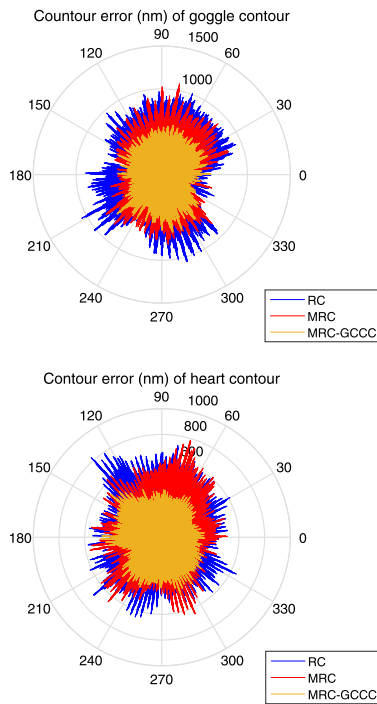


FIGURE 13. Experimental results of MRC-GCCC (goggle contour (top), heart contour (bottom)).

$\alpha = 0.999$ . The experimental results are shown in FIGURE 12 and 13, where it is seen that the MRC-CCC/GCCC outperformed the standalone RC and MRC. The comparison of the contour errors with MRC of three types of references was summarized in TABLE 6.

To better compare the experimental results, we collect the contour errors (in RMS values) in bar charts shown in FIGURE 14 and 15. It is seen from FIGURE 14 that the proposed RC-CCC/GCCC method outperformed the standalone

TABLE 6. The experimental contour errors (nm) with MRC.

Contour	MRC	MRC-CCC/GCCC	Error reduction
Circular contour	186.8	102.8	45.0%
Goggle contour	291.6	214.1	26.6%
Heart contour	182.8	149.3	18.3%

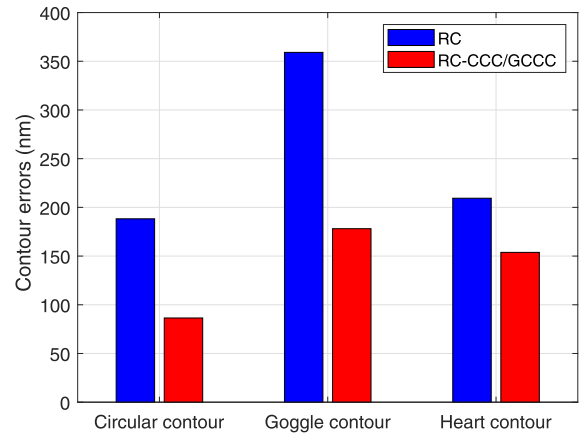


FIGURE 14. Comparison of experimental contour errors (RMS) between RC and RC-CCC/GCCC.

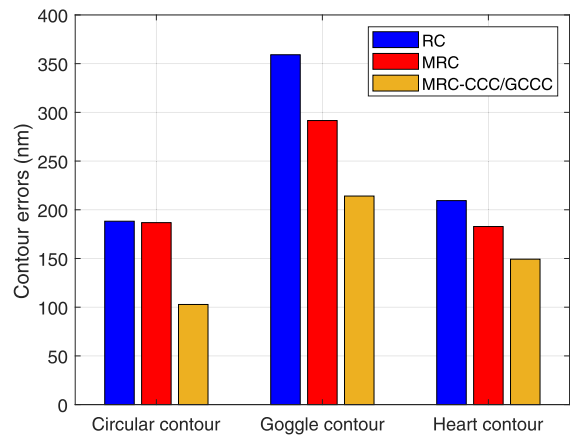


FIGURE 15. Comparison of experimental contour errors (RMS) between RC, MRC and MRC-CCC/GCCC.

RC for regular and free form contours. Similarly FIGURE 15 shows that the proposed MRC-CCC/GCCC method outperformed the standalone RC and MRC for regular and free form contours.

V. CONCLUSION

For the purpose of microfabrication and simple implementation for an MSL system, we have proposed a novel integrated RC and CCC structure to achieve high precision contouring control. The proposed control structure is composed of the RC and CCC as the axial periodic tracking controller and the contour error coordination controller, respectively. To achieve an effective integration of RC and CCC, the contour error feedback position is crucial as an incorrect one might even deteriorate the contouring. We have designed a

correct feedback position, and constructed a cross-coupled controller to ensure the stability and contour error reduction for the proposed control structure. Various simulation and experimental scenarios are deployed on a self-developed XY nanomanipulator. And the comparative results validate that the proposed control method outperformed non-integrated ones by achieving nanometric contour tracking with the contour error 86 nm.

## APPENDIX PROOF OF THEOREM 1

*Proof:* To show the stability of the proposed RC-CCC method, it is sufficient [33] to show that both the axial RC controller and equivalent CCC control system are stable. The stability of RC is referred to [34], then it is left to show the stability of the equivalent CCC system.

Define the equivalent CCC structure between the uncoupled RC and coupled RC as follows: define  $\varepsilon_c$  as the contour error of the RC-CCC, and  $\varepsilon_u$  as the contour error of the uncoupled RC. Then the following result holds [33],

$$\varepsilon_c = \frac{1}{1 + CK} \varepsilon_u, \quad (17)$$

where  $K$  is of the form

$$K(z^{-1}) = \frac{(1 + K_{p_x} P_{c_x}) C_y^2 P_{c_y} + (1 + K_{p_y} P_{c_y}) C_x^2 P_{c_x}}{(1 + K_{p_x} P_{c_x})(1 + K_{p_y} P_{c_y})}. \quad (18)$$

Notice that in the RC-CCC structure,

$$K_{p_i}(z^{-1}) = \frac{z^{-(N-r)}}{1 - z^{-N}}, \quad i = x, y, \quad (19)$$

$$P_{c_i}(z^{-1}) = K_{r_i} P_{ZPET_i}(z^{-1}) P_{n_i}(z^{-1}), \quad i = x, y. \quad (20)$$

Substituting equations (2), (9) and (14) into equation (20), which yields

$$P_{c_i}(z^{-1}) = z^{-r} S_i(z^{-1}), \quad i = x, y. \quad (21)$$

The open loop transfer function of the equivalent CCC system is  $CK$ , of which the poles are calculated based on the following characteristic equation

$$W_x(z^{-1}) \cdot W_y(z^{-1}) \cdot (1 - z^{-N}) = 0, \quad (22)$$

by noting equations (12), (18)-(21). Also  $W_i(z^{-1}) = 0$  is the closed loop characteristic equation of RC, with roots all inside the unit circle. Thus, there is no pole of the open loop transfer function of the equivalent CCC system outside the unit circle.

The amplitude frequency response of the open loop transfer function is of the form

$$\left| CK(e^{-j\omega}) \right| = \frac{k_c}{C_x^2 + C_y^2} \left| C_y^2 e^{-j\omega r} S_y(e^{-j\omega}) W_x(e^{-j\omega}) + C_x^2 e^{-j\omega r} S_x(e^{-j\omega}) W_y(e^{-j\omega}) \right|. \quad (23)$$

For the RC, it is noted that  $|S_i(e^{-j\omega})| < 2$ , and  $|W_i(e^{-j\omega})| \leq |e^{-j\omega N} [S_i(e^{-j\omega}) - 1]| + 1 < 2$ . Substitute the above inequalities into equation (23), yielding

$$\left| CK(e^{-j\omega}) \right| < \frac{4C_y^2 + 4C_x^2}{(C_x^2 + C_y^2)/k_c} < 4k_c < 1. \quad (24)$$

The above inequality implies in the Nyquist plot, there is no encirclement of point  $(-1, 0)$ . Therefore the equivalent CCC system is stable, and so is the RC-CCC system.  $\square$

## REFERENCES

- [1] K. Ikuta and K. Hirowatari, "Real three dimensional micro fabrication using stereo lithography and metal molding," in *Proc. IEEE Micro Electro Mech. Syst.*, Fort Lauderdale, FL, USA, Dec. 2002, pp. 42–47.
- [2] T. Takagi and N. Nakajima, "Photoforming applied to fine forming," *JSME Int. J. C, Dyn., Control, Robot., Design Manuf.*, vol. 38, no. 4, pp. 811–817, 1995.
- [3] H. Lin, D. Zhang, P. G. Alexander, G. Yang, J. Tan, A. W.-M. Cheng, and R. S. Tuan, "Application of visible light-based projection stereolithography for live cell-scaffold fabrication with designed architecture," *Biomaterials*, vol. 34, no. 2, pp. 331–339, Jan. 2013.
- [4] A. K. Miri, D. Nieto, L. Iglesias, H. Goodarzi Hosseinabadi, S. Maharjan, G. U. Ruiz-Esparza, P. Khoshakhlagh, A. Manbachi, M. R. Dokmeci, S. Chen, S. R. Shin, Y. S. Zhang, and A. Khademhosseini, "Microfluidics-enabled multimaterial maskless stereolithographic bioprinting," *Adv. Mater.*, vol. 30, no. 27, Jul. 2018, Art. no. 1800242.
- [5] H.-W. Kang, I. H. Lee, and D.-W. Cho, "Development of an assembly-free process based on virtual environment for fabricating 3D microfluidic systems using microstereolithography technology," *J. Manuf. Sci. Eng.*, vol. 126, no. 4, pp. 766–771, Nov. 2004.
- [6] C. L. Petersen, R. Lin, D. H. Petersen, and P. F. Nielsen, "Micro-scale sheet resistance measurements on ultra shallow junctions," in *Proc. 14th IEEE Int. Conf. Adv. Ther. Process. Semiconductors*, Kyoto, Japan, Oct. 2006, pp. 153–158.
- [7] B. A. Wester, S. Rajaraman, J. D. Ross, M. C. Laplaca, and M. G. Allen, "Development and characterization of a packaged mechanically actuated microtweezer system," *Sens. Actuators A, Phys.*, vol. 167, no. 2, pp. 502–511, Jun. 2011.
- [8] S. Maruo and S. Kawata, "Two-photon-absorbed near-infrared photopolymerization for three-dimensional microfabrication," *J. Microelectromech. Syst.*, vol. 7, no. 4, pp. 411–415, 1998.
- [9] S. Kawata, H.-B. Sun, T. Tanaka, and K. Takada, "Finer features for functional microdevices," *Nature*, vol. 412, no. 6848, pp. 697–698, Aug. 2001.
- [10] S. Maruo and K. Ikuta, "Three-dimensional microfabrication by use of single-photon-absorbed polymerization," *Appl. Phys. Lett.*, vol. 76, no. 19, pp. 2656–2658, May 2000.
- [11] M. Thiel, J. Fischer, G. Von Freymann, and M. Wegener, "Direct laser writing of three-dimensional submicron structures using a continuous-wave laser at 532 nm," *Appl. Phys. Lett.*, vol. 97, no. 22, Nov. 2010, Art. no. 221102.
- [12] H.-W. Kang, Y.-S. Jeong, S.-J. Lee, K.-S. Kim, and W.-S. Yun, "Development of a compact micro-stereolithography (MSTL) system using a Blu-ray optical pickup unit," *J. Micromech. Microeng.*, vol. 22, no. 11, Nov. 2012, Art. no. 115021.
- [13] J.-H. Kim, J. W. Lee, and W.-S. Yun, "Fabrication and tissue engineering application of a 3D PPF/DEF scaffold using Blu-ray based 3D printing system," *J. Mech. Sci. Technol.*, vol. 31, no. 5, pp. 2581–2587, May 2017.
- [14] C. W. Hull, "Apparatus for production of three-dimensional objects by stereolithography," U.S. Patent 4 575 330, Mar. 11, 1986.
- [15] Z. Liu, Z. Zhang, and Y. Guan, "Development of a compact and cost effective MSL system based on a compliant nanomanipulator," in *Proc. 15th IEEE/ASME Int. Conf. Mech. Embedded Syst. Appl.*, Anaheim, CA, USA, vol. 9, Aug. 2019, p. 97522.
- [16] P. Ouyang and T. Dam, "Position domain PD control: Stability and comparison," in *Proc. IEEE Int. Conf. Inf. Autom.*, Shenzhen, China, Jun. 2011, pp. 8–13.
- [17] T. Dam and P. Ouyang, "Position domain contour tracking with cross-coupled control," in *Proc. IEEE Int. Symp. Ind. Electron.*, Hangzhou, China, May 2012, pp. 1303–1308.
- [18] G.-C. Chiu and M. Tomizuka, "Contouring control of machine tool feed drive systems: A task coordinate frame approach," *IEEE Trans. Control Syst. Technol.*, vol. 9, no. 1, pp. 130–139, Jan. 2001.
- [19] C. Hu, Z. Wang, J. Chen, Y. Zhu, and M. Zhang, "Generalized GTCF coordination mechanism based LARC contouring control of industrial motion stages for complex contours," *IEEE Access*, vol. 6, pp. 20067–20076, 2018.

- [20] Z. Chen, C. Li, B. Yao, M. Yuan, and C. Yang, "Integrated coordinated/synchronized contouring control of a dual-linear-motor-driven gantry," *IEEE Trans. Ind. Electron.*, to be published, doi: 10.1109/tie.2019.2921287.
- [21] Y. Koren and C.-C. Lo, "Variable-gain cross-coupling controller for contouring," *CIRP Ann.*, vol. 40, no. 1, pp. 371–374, 1991.
- [22] J. Lee, W. E. Dixon, and J. C. Ziegert, "Adaptive nonlinear contour coupling control for a machine tool system," *Int. J. Adv. Manuf. Technol.*, vol. 61, nos. 9–12, pp. 1057–1065, Aug. 2012.
- [23] J. Yao, X. Cao, Y. Zhang, and Y. Li, "Cross-coupled fuzzy PID control combined with full decoupling compensation method for double cylinder servo control system," *J. Mech. Sci. Technol.*, vol. 32, no. 5, pp. 2261–2271, May 2018.
- [24] K. Barton and A. Alleyne, "A cross-coupled iterative learning control design for precision motion control," *IEEE Trans. Control Syst. Technol.*, vol. 16, no. 6, pp. 1218–1231, Nov. 2008.
- [25] L. Sheng, G. Xiaojie, and Z. Lanyong, "Robust adaptive backstepping sliding mode control for six-phase permanent magnet synchronous motor using recurrent wavelet fuzzy neural network," *IEEE Access*, vol. 5, pp. 14502–14515, 2017.
- [26] J. Liao, Z. Chen, and B. Yao, "Performance-oriented coordinated adaptive robust control for four-wheel independently driven skid steer mobile robot," *IEEE Access*, vol. 5, pp. 19048–19057, 2017.
- [27] Y. Cao and Z. Zhang, "Cross-coupled repetitive control of an XY compliant nanomanipulator," in *Proc. 37th Chin. Control Conf. (CCC)*, Wuhan, China, Jul. 2018, pp. 8154–8159.
- [28] Z. Zhang, P. Yan, and G. Hao, "A large range flexure-based servo system supporting precision additive manufacturing," *Engineering*, vol. 3, no. 5, pp. 708–715, Oct. 2017.
- [29] Y. Koren, "Cross-coupled biaxial computer control for manufacturing systems," *J. Dyn. Syst., Meas., Control*, vol. 102, no. 4, pp. 265–272, Dec. 1980.
- [30] F. Huo and A.-N. Poo, "Improving contouring accuracy by using generalized cross-coupled control," *Int. J. Mach. Tools Manuf.*, vol. 63, pp. 49–57, 2012.
- [31] X. Chen and M. Tomizuka, "New repetitive control with improved steady-state performance and accelerated transient," *IEEE Trans. Control Syst. Technol.*, vol. 22, no. 2, pp. 664–675, Mar. 2014.
- [32] M.-Y. Cheng, K.-H. Su, and S.-F. Wang, "Contour error reduction for free-form contour following tasks of biaxial motion control systems," *Robot. Comput.-Integr. Manuf.*, vol. 25, no. 2, pp. 323–333, Apr. 2009.
- [33] S.-S. Yeh and P.-L. Hsu, "Theory and applications of the robust cross-coupled control design," in *Proc. IEEE Amer. Control Conf.*, Albuquerque, NM, USA, vol. 1, Jun. 1997, pp. 791–795.
- [34] M. Tomizuka, T.-C. Tsao, and K.-K. Chew, "Discrete-time domain analysis and synthesis of repetitive controllers," in *Proc. Amer. Control Conf.*, Atlanta, GA, USA, Jun. 1988, pp. 860–866.



**YUE CAO** (Student Member, IEEE) received the B.S. degree in mechanical engineering from the Department of Mechanical Engineering, Tsinghua University, Beijing, China, in 2018, where he is currently pursuing the Ph.D. degree in mechanical engineering.

His current research interests include modeling and control of micro-/nano-precision mechatronic systems and applications in advanced manufacturing. He was a recipient of the IEEE International Conference on Manipulation, Manufacturing and Measurement on the Nanoscale Best Application Paper Award, in 2019.



**ZHEN ZHANG** (Member, IEEE) received the B.S. degree from Shanghai Jiao Tong University, Shanghai, China in 1998, the M.S. degrees from Tsinghua University, Beijing, China, in 2001, and Vanderbilt University, Nashville, TN, USA, in 2003, and the Ph.D. degree in electrical and computer engineering from The Ohio State University, Columbus, OH, USA, in 2007.

From 2007 to 2009, he was a Postdoctoral Fellow with the Mechanical Engineering Department, University of Minnesota. Since 2009, he has been with the Faculty of the Department of Mechanical Engineering, Tsinghua University. His research interests include design, modeling and control of micro-/nano-precision mechatronic systems and applications in advanced manufacturing (e.g., ultrafast laser processing).

Prof. Zhang was a recipient of the IEEE International Conference on Manipulation, Manufacturing and Measurement on the Nanoscale Best Application Paper Award, in 2019. He is also the Topical Editor of the journal *Mechanical Sciences*.

• • •